Antibacterial performance of hybrid nanocomposite coatings containing clay and silver nanoparticles

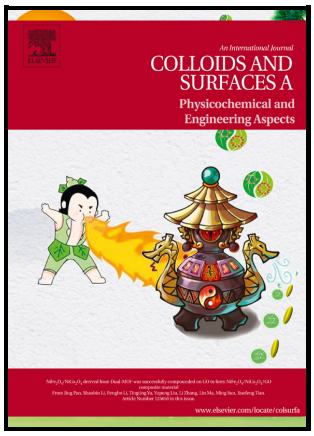

Hugo F. Giraldo Mejía, Karina Herrera Seitz, Matías Valdés, Abdusalam Uheida, Raúl A. Procaccini, Sergio A. Pellice

PII: S0927-7757(21)01223-1

DOI: https://doi.org/10.1016/j.colsurfa.2021.127354

Reference: COLSUA127354

To appear in: *Colloids and Surfaces A: Physicochemical and Engineering Aspects*

Received date: 30 April 2021
Revised date: 6 August 2021
Accepted date: 8 August 2021

Please cite this article as: Hugo F. Giraldo Mejía, Karina Herrera Seitz, Matías Valdés, Abdusalam Uheida, Raúl A. Procaccini and Sergio A. Pellice, Antibacterial performance of hybrid nanocomposite coatings containing clay and silver nanoparticles, *Colloids and Surfaces A: Physicochemical and Engineering Aspects,* (2021) doi:https://doi.org/10.1016/j.colsurfa.2021.127354

Antibacterial performance of hybrid nanocomposite coatings containing clay and silver nanoparticles

Hugo F. Giraldo Mejía *[1, †3], *Karina Herrera Seitz* [2], *Matías Valdés* [3], *Abdusalam Uheida* [4], *Raúl A. Procaccini* [3], *Sergio A. Pellice* [3].

[1] Advanced Mining Technology Center (AMTC), Universidad de Chile, Av. Tupper 2007, 8370451 Santiago, Chile.

[2] Instituto de Investigaciones Biológicas (IIB), Grupo Quimiotaxis, CONICET-UNMdP, Funes 3250, 7600 Mar del Plata, Argentina.

[3] Instituto de Investigación en Ciencia y Tecnología de Materiales (INTEMA), CONICET-UNMdP, Av. Colón 10850, 7600 Mar del Plata, Argentina.

[4] Functional Materials group, Department of Applied Physics, School of Engineering Sciences, KTH Royal Institute of Technology, Hannes Alfvéns väg 12, 114 19 Stockholm, Sweden.

Keywords: Synchrotron SAXS; Laponite; Silver releasing; E. coli; Biocide coating.

ABSTRACT. The performance of biocide-based coatings for health care applications, using the drug delivery method, depends primarily on the diffusive properties of storage material. When the active component is ionic silver, supplied from silver nanoparticles, an additional dissolution step must occur in the bulk of the storage material. This article presents the silver release behavior of organic-inorganic sol-gel hybrid coatings and the effect of clay-nanoparticle

composite, added in the sol-type formulation. Hybrid coatings were synthesized from the hydrolytic condensation of (3-glycidoxypropyl)-trimethoxysilane (GPTMS) and tetraethoxysilane in acidic media. Clay nanoparticles, previously silanized with GPTMS, and silver nitrate were used as additives in sol-gel formulations, alternatively. Coatings were deposited on microscope glass slides by the dip-coating process at a constant withdrawal rate and densified at 150 °C. Through small angle X-ray scattering from a synchrotronic source, and transmission electron microscopy, the structure of hybrid matrix, silver nanoparticles morphology and the storability behavior of silver nanoparticles under leaching conditions was analyzed. Silver releasing process was analyzed by following the evolution of silver nanoparticles remaining in the coatings, by UV-visible spectroscopy, and the increase of silver ions in the liquid medium, using inductively coupled plasma with optical emission spectroscopy. Microbiological studies showed that the lixiviated silver exhibited inhibitory properties against *E. coli* in LB broth. The clay nanoparticles worked as a stabilizing agent avoiding the agglomeration of silver both on the sols and on the surface of the thermally densified coatings.

1. INTRODUCTION

Population density is increasing worldwide and, as a result, social infrastructures such as public transportation, educational and health facilities, and sports and recreational facilities are being used more intensively. This phenomenon brings to an even more frequent exposure of people to an innumerable variety of pathogenic microorganisms. Such complex scenario leads the society to adopt different strategies to address the public health problem and minimize the propagation of infectious diseases. Commonly, hazardous microorganisms are spread in the population

through physical contact with contaminated surfaces, where bacteria can persist or even grow unrestricted.

Silver ions are well-known for their biocidal properties, which inhibit the development of many bacteria, fungi and viruses [1–4]. This property allows the development of many materials and devices capable of improving the health conditions of population by limiting the growth of dangerous microorganisms on surfaces exposed to human contact. The effectiveness of silver-based biocidal materials depends on their ability to efficiently supply silver ions or small clusters [5–12]. Through an oxidative dissolution process, silver nanoparticles can provide these Ag^{+} ions. Certainly, the smaller the silver nanoparticles, the higher the surface reactivity and antibacterial properties [13,14].

Nevertheless, to ensure the maximum benefit of this kind of biocide ion supply mechanism, the silver nanoparticles must be contained in a matrix material whose nanostructure allows a smooth diffusion of all the reagents involved in their chemical reactions. Hybrid organic-inorganic materials are capable of exhibiting a phase separation structure, in which the organic and inorganic components are immiscible with each other. Thus, organometallic precursors, such as the organically modified alkoxysilanes, are molecules whose organic and inorganic components could give rise to materials with two interpenetrating phases, whose reticular nanostructures provide a desired combination of mechanical and diffusive properties. Epoxy networks are well-known for their hygroscopic characteristics and high performance in structural devices [15–17]; then, its chemical structure seems a good choice to be the water permeable organic phase allowing the diffusion of the necessary reagents to enable the desired supply of silver ions.

Nonetheless, in order to be considered for industrial or healthcare applications, silver-based biocidal coatings must achieve optimal diffusive and mechanical properties. The ionic mobility of silver could be extremely fast within organic phases of hybrid materials, providing a strong antibacterial behavior, but only in the short term [18–20]. Clay nanosheets are a reliable component to successfully control silver nanoparticle size and then ionic release performance [21]. Furthermore, the use of clay nanoparticles is known to improve the mechanical, structural and barrier properties of epoxy-clay based composites [22–24]. On the other hand, taking into account that nanoclays have crystalline structures in form of 1 nm thick platelets, they are a clear alternative as a key component for the development of functional thin coatings with straight dimensional limitations [25–27].

In this work, the evolution of silver nanoparticles under water immersion conditions was analyzed in relation to the presence of clay nanoparticles in hybrid organic-inorganic coatings. Likewise, these results were contrasted with the relationship between the silver release process and the antibacterial activity of the coatings. Hybrid coatings were synthesized, as described in a previous work [28], from the hydrolytic condensation of 3-(glycidoxypropyl)-trimethoxysilane (GPTMS) and tetraethoxysilane (TEOS) in a molar ratio 40/60, respectively. Clay nanoparticles were introduced in a 2 wt. %, in respect to the hydrolytically condensed silica. Its stability in the sol stage, with and without silver ions, was analyzed through dynamic light scattering (DLS). The effect of clay nanoparticles on the surface morphology of coatings and on the formation of silver aggregates on coatings surfaces was analyzed using field emission scanning electron microscopy (FESEM). The performance of the hybrid organic-inorganic matrix, as a permeable nanostructure capable of retaining silver nanoparticles within its bulk material and allowing ionic release of silver, was analyzed through small angle X-ray scattering (SAXS) from a synchrotron

light source. The silver release was monitored under water immersion conditions by analyzing lixiviated and remaining silver through inductively coupled plasma with optical emission spectrometry (ICP-OES) and UV-visible spectroscopy, respectively. Finally, the microbiological behavior under immersion conditions in nutrients-rich water was analyzed against *E. coli* cultures.

2. EXPERIMENTAL

2.1. Materials and samples preparation

Hybrid sols were obtained under a procedure previously described [28]. Clay nanoparticles (Laponite® S482) were dispersed in aqueous-ethanolic media and were exposed to a grafting process with 3-glycidoxypropyl-trimethoxysilane (GPTMS, Aldrich 99 %) under ultrasonic agitation and neutral pH. The resulting grafted nanoclay suspension was then mixed with tetraethoxysilane (TEOS, Aldrich 98 %) keeping a molar ratio of GPTMS/TEOS = 40/60 and 2 wt. % of clay, relative to condensed silica. Hydrolytic condensation of the alkoxy groups of the unreacted GPTMS and TEOS, and the opening of epoxy rings, was performed by the addition of concentrated nitric acid (HNO_3) under vigorous magnetic stirring at 1200 rpm and 25 °C. Ag^+ ions were further added, at a molar ratio Ag/Si = 3/97, from an ethanolic solution previously prepared using silver nitrate ($AgNO_3$) and pyridine as stabilizer. For comparative purposes, sols without clay nanoparticles and without silver doping were synthetized alternatively. So, four kinds of precursor sols were obtained: a basis matrix sol from TEOS and GPTMS (TG), a basis sol with clay nanoparticles (TGL), a basis sol with clay nanoparticles and silver doping (TGL-Ag) and a basis sol with silver doping (TG-Ag). The hybrid coatings were obtained by an dip-coating process on soda-lime glass microscope slides, and exposed to a thermal consolidation at

150 °C during 30 minutes in air atmosphere. Figure 1 displays a representative scheme corresponding to the process of synthesis for TGL and TGL-Ag coatings, where T is temperature, t is time and ν is ultrasonic stirring.

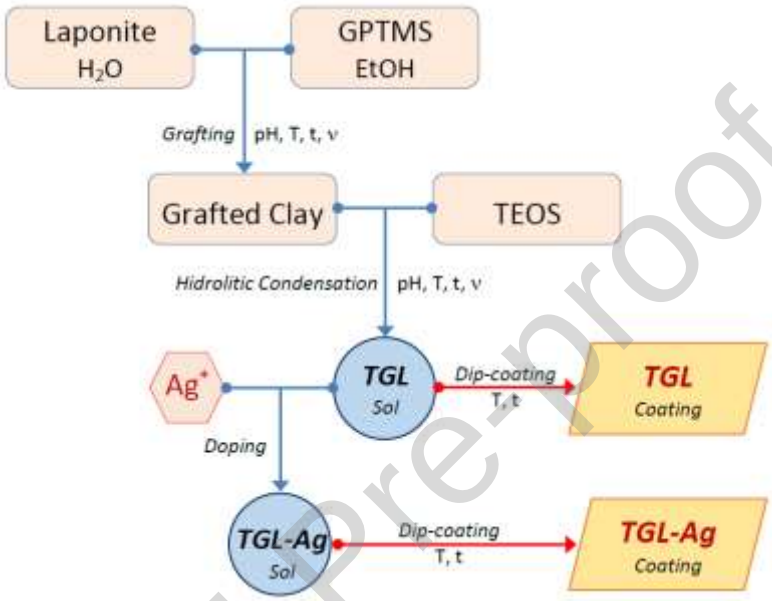

Figure 1. Schematic diagram of the synthesis process for TGL and TGL-Ag coatings.

2.2. Dynamic Light Scattering

To study the characteristics and stability of the particles involved in the clay silanization and hydrolytic condensation stages, dynamic light scattering (DLS) analysis, also known as photon correlation spectroscopy or quasi-elastic light scattering, was performed. Samples were previously exposed to an ultrasonic dispersion process at 80 W for 10 minutes and filtered through PTFE membrane syringe filters with pore size of 0.45 micrometer, in order to remove agglomerated particles. The hydrodynamic radius and size distribution of the nanoparticles were determined at 21 °C in a threefold acquisition process using a transparent cuvette with a sample volume of 1 mL (ZETASIZER Nano-Series, Nano-S90).

2.3. Electron microscopy

Surface morphology of coatings was observed through Scanning Electron Microscopy (FE-SEM, Neon Zeiss 40, Germany). Morphology of silver nanoparticles enclosed in hybrid organic-inorganic coatings was observed through Transmission Electron Microscopy (TEM, JEOL 100CX II, Japan). Hybrid coatings were detached from glass substrates through mechanical scratching and milled in an agate mortar; powdered samples were dispersed in ethanol and deposited on 200-mesh formvar-coated grids.

2.4. Synchrotron SAXS

The structural properties of the hybrid matrix and distribution of silver nanoparticles were analyzed by Small Angle X-ray Scattering (SAXS). The experiments were carried out using the SAXS1 beamline of the National Laboratory of Synchrotron Light (LNLS, Campinas, Brazil). Coatings were taken out from glass substrates by scratching. The resulting glassy powder was placed in the sample holders by an adhesive polyimide film (Kapton®, DuPont). In order to subtract the contribution of the adhesive tape from SAXS patterns, Kapton® film was used as background. The collimated beam crossed the samples through an evacuated flight tube and was scattered to 2D bump-bonded hybrid-pixel Pilatus detector with an active area of 28 cm^2 and pixel size of 172 × 172 μm^2. The geometrical configuration was set up with the sample detector distance of 473.5 mm with monochromatic light of λ = 1.55 Å. The q range was calibrated with silver behenate ($CH_3(CH_2)_{20}COOAg$), which has a well-known lamellar structure with d = 5.848 nm [29]. The isotropic 2D scattering patterns were collected after exposure times of 10 s. Images were corrected considering the detector dark noise and normalized by the sample transmission

considering the 360 azimuthal scans. This procedure was carried out using the FIT2D software [30]. SAXS data were processed by the SASfit software package [31].

The hybrid organic-inorganic matrix was fitted with a combination of two form factors developed for bi-continuous systems: the Teubner-Strey (TS) and the Debye-Anderson-Brumberger (DAB) models. On the other hand, the presence of silver nanoparticles was fitted according to spherical nanoparticles following a Schultz-Zimm (SZ) size distribution.

The TS phenomenological model accurately describes scattering from bi-continuous micro-emulsions [32]. The scattered intensity for TS model is given by Eq.1:

$$I_{TS}(q) = \frac{8\pi\langle\eta^2\rangle/\xi}{a^2-2bq^2+q^4} \qquad \text{Eq. 1}$$

where $a^2 = (k^2 + 1/\xi^2)^2$ and $b = k^2 - 1/\xi^2$; k is defined as $2\pi/d$ and d represents a quasi-periodic repeat distance between the two-phases regions. The correlation length ξ corresponds to a characteristic length for positional correlation. The scattering curves of bi-continuous microemulsions present a peak at $q = b^{1/2}$. On the other hand, the DAB form factor model, Eq. 2, calculates the scattering from a randomly distributed, non-particulate, two-phase system [33]. The two-phase system is characterized by a single length scale, d, which is a measure of the average spacing between regions of phase 1 and phase 2. This model also assumes smooth interfaces between the phases and hence exhibits Porod behavior ($I \propto q^{-4}$) at large q values. The macroscopic scattering cross-section in the DBA model is given by:

$$I_{DAB}(q) = I_0 \frac{1}{[1+(qd)^2]^2} \qquad \text{Eq. 2}$$

The SZ size distribution (Eq. 3), derived from thermodynamic theories, is particularly important and has a better match to reality than the normal Gaussian distribution to describe particles distribution [34].

$$SZ(R, N, R_a, k) = \frac{N}{R_a}\left(\frac{R}{R_a}\right)^{k-1} \frac{k^k e^{-kR/Ra}}{\Gamma(k)} \quad \text{Eq. 3}$$

where the parameter k of the size distribution is related to the variance σ by $k = 1/\sigma^2$. R_a is the scaling parameter and defines the maximum of the size distribution for large values of k.

2.5. UV-visible spectroscopy

The evolution of the plasmonic bands during the lixiviation process was followed with an ultraviolet-visible spectrophotometer (UV-Vis-NIR, Shimadzu 3600Plus) equipped with integrating sphere. Spectra were recorded in absorbance mode in the 200-1000 nm wavelength range, with a resolution of 1 nm, using barium sulphate ($BaSO_4$) as the reflexivity standard. The samples, consisting of described coatings (TGL and TGL-Ag) on slides, were placed inside the integrating sphere to perform the spectra at room temperature.

2.6. ICP measurements

Inductively Coupled Plasma Optical Emission Spectrometry (Thermo Scientific ICP-OES - iCAP 6500), provided with a solid-state swing frequency RF plasma generator, was used in the measurement of total silver content in aqueous samples leached at different immersion times. The spectrometer is equipped with an Innovative Charge Injection Device (CID) detector, CID-86 with continuous choice of wavelengths in the range 166 to 847 nm. Data acquisition was performed with iTEVA software suite. Glass slides with 12 cm^2 of coating were immersed in 250 mL of deionized water and samples were periodically collected during the leaching process

over 8 h and analyzed. The leaching processes were followed by triplicate determinations on leachate samples at different times from TG-Ag and TGL-Ag coatings at 20 and 37 °C.

2.7. Microbiological tests

Antibacterial performance against *E. coli* cultures was quantitatively analyzed to determine the effect of incorporating clay nanoparticles in silver-enriched coatings. Glass samples of 6 cm^2, coated with TG, TGL, TG-Ag or TGL-Ag sols, were immersed in 5 mL of LB broth (10 g/l tryptone, 5 g/l yeast extract, 5 g/l NaCl) inoculated with *E. coli* cultures (K12 strain RP437) and incubated at 37 °C in a rotatory shaker (200rpm). The initial bacterial concentrations, measured in colony forming units (CFU), were between 10^6 and 10^9 CFU/mL. Bacterial growth was followed through three-fold determinations of the optical density (OD) values obtained at λ = 600 nm.

3. RESULTS AND DISCUSSION

The synthesis process involved in the development of the hybrid coatings, including those containing clay, made it possible to obtain transparent sols for each composition studied. Only in TG-Ag sol, without clay nanoparticles, a very slight brownish coloration was observed. As described in a previous work, clay nanoparticles induce a stabilizing effect on the agglomeration process of silver ions, minimizing the growing of particles both in sol and gel stages [28]. DLS studies showed the development of a monomodal hydrodynamic size distribution of silanized clay nanoparticles, which did not undergo any destabilizing effect with the incorporation of the ionic silver solution. While the average hydrodynamic size of clay nanoparticles was of 123.7 ± 12.8 nm, for TGL sol, the results for silver containing sols, TGL-Ag, showed a size of 122.1 ± 12.2 nm.

After the drying and thermal densification process of the coatings, silver ions underwent an agglomeration process leading to the development of silver nanoparticles embedded in the hybrid organic-inorganic structure. This phenomenon caused a turning brown of silver-containing coatings; TG-Ag and TGL-Ag formulations. Since the antibacterial effect of silver nanoparticles is based in their ability to deliver silver ions, *e.g.*, by reacting silver nanoparticles in an oxidative dissolution process [35–40]. Then, the way the silver nanoparticles were stored in a coating will have strong effect on the ionic silver releasing and the resulting biocidal properties of coatings.

3.1. Hybrid structure and silver nanoparticle storage

The confinement of silver nanoparticles in a solid environment, allowing subsequent free mobility of silver ions, is essential to achieve the desired long-term antibacterial performance. TEM micrograph of TG-Ag sample is shown in Figure 2. As can be observed in the image, spherical silver nanoparticles, developed from Ag^{+} ions in a thermal process, are embedded in the hybrid organic-inorganic matrix. Due to the solid state of both the silver nanoparticles and the highly crosslinked polymeric network of the surrounding sol-gel matrix, these silver nanoparticles are unable to be released to the external environment in such agglomerated state.

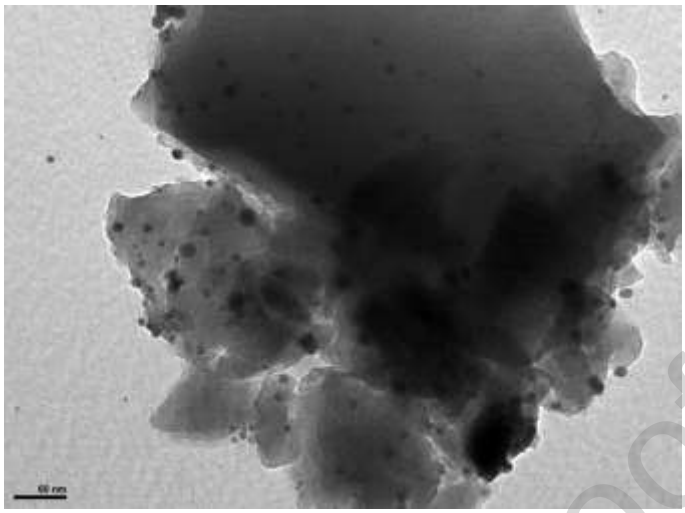

Figure 2. TEM image of the TG-Ag sample. Spherical silver nanoparticles are observed, embedded in the bulk of the hybrid matrix (Mag. 200000 X; scale bar: 60 nm)

Thus, to achieve an effective silver releasing process, the hybrid sol-gel network should be enough open to allow the free movement of ionic species and small clusters. Considering that the silver releasing process is mainly related to diffusivity and surface reaction of silver nanoparticles, an important factor to be taken into consideration is the three-dimensional structure of the hybrid organic-inorganic sol-gel matrix through which silver ions, oxygen, and water (products and reagents) might diffuse.

Synchrotron radiation facilities permit the study of exceedingly small structural components present within nanometric complex scenarios such as these hybrid samples analyzed here. Figure 3 *a* shows the small angle X-ray scattering curves, recorded in the range 0.24 $nm^{-1} \leq q \leq 5.3$ nm^{-1}, of TG-Ag sample before and after a lixiviation process of 24 h at 37 °C in DI water. The analyzed region allows to determine, on the one hand, the size distribution of the smallest silver nanoparticles present in the material and, on the other hand, the structural morphology corresponding to the hybrid organic-inorganic matrix. SAXS curve of TG sample, without silver

loading, shows a single shape composed of just a straight line, with a slope of -4, and a wide peak at q = 3.7 nm^{-1}. This curve could be fitted by simply using a two-component system: a Teubner-Strey (TS) and a Debye-Anderson-Brumberger (DAB) models of form factors [33]. DAB model calculates the scattering from a randomly distributed, non-particulate, two-phase system and also assumes smooth interfaces between the phases and hence exhibits Porod behavior ($I \propto q^{-4}$) at large q values. Moreover, the TS model describes the scattering process of inhomogeneous materials with a bi-continuous spinodal-like phase separation or bi-continuous microemulsion structures [32,41,42]. The bi-continuous structure is characteristic of hybrid organic-inorganic sol-gel materials, where the organic and inorganic components are covalently bonded and a spinodal-like phase separation between silica-rich and organic-rich domains results in a narrow pore size distribution of the silica network [19,43,44]. The position of the peak, observed in all the samples, is associated to a characteristic length given by $2\pi/q$ = 1.7 nm; this length, coincidently, approaches to the double of the size of the organic component of GPTMS. The presence of this bi-continuous structure could be highly advantageous to enable an effective permeability and then, to allow the oxidative dissolution of silver nanoparticles to proceed adequately and also silver ions to reach the coating surface and act against microorganisms.

The evolution of silver nanoparticles within the sol-gel structure can also be analyzed using synchrotron SAXS. The shoulders below q = 2 nm^{-1}, present in SAXS curves of TG-Ag samples, are characteristic of materials with spherical nanoparticles present with a polydisperse size distribution. Undoubtedly, these nanoparticles are silver, previously observed by electron microscopy. Since these nanoparticles developed from the ionic silver, incorporated into the material during the sol stage, it is to be expected that they are present in a wide size distribution, from small clusters to those readily observable through TEM.

Figure 3 *b* shows the results of SAXS curve fittings of TG-Ag sample. Prior to lixiviation process, a Schultz-Zimm size distribution of particles with R_a = 2.23 nm, σ = 0.56 nm, and the maximum at 1.52 nm of radius was obtained. It can be observed that asymmetric size distribution curve broadly shifted towards the smaller sizes but with a slight intensity up to particles of ~15 nm of radius, as these seen through TEM. After a lixiviation process of 24 h immersion in DI water, the SAXS curve fitting evidenced the losing of near the totally of particles smaller than ~2 nm of radius. In this case, the fitting procedure gave values of R_a = 3.46 nm and σ = 0.23 nm, with its maximum at 3.26 nm of radius. Although the configuration used for the SAXS experiments does not allow determining the presence of larger silver nanoparticles in the coatings, it can be assured that they can hardly be removed from the hybrid organic-inorganic nanostructure without a dissolution process. In our previous work, determination of silver nanoparticles size was performed using Debye-Scherrer analysis on XRD spectra [28], and the obtained size of silver nanoparticles in TG-Ag and TGL-Ag samples were 28.4 ± 2.8 nm and 21.5 ± 2.2 nm, respectively.

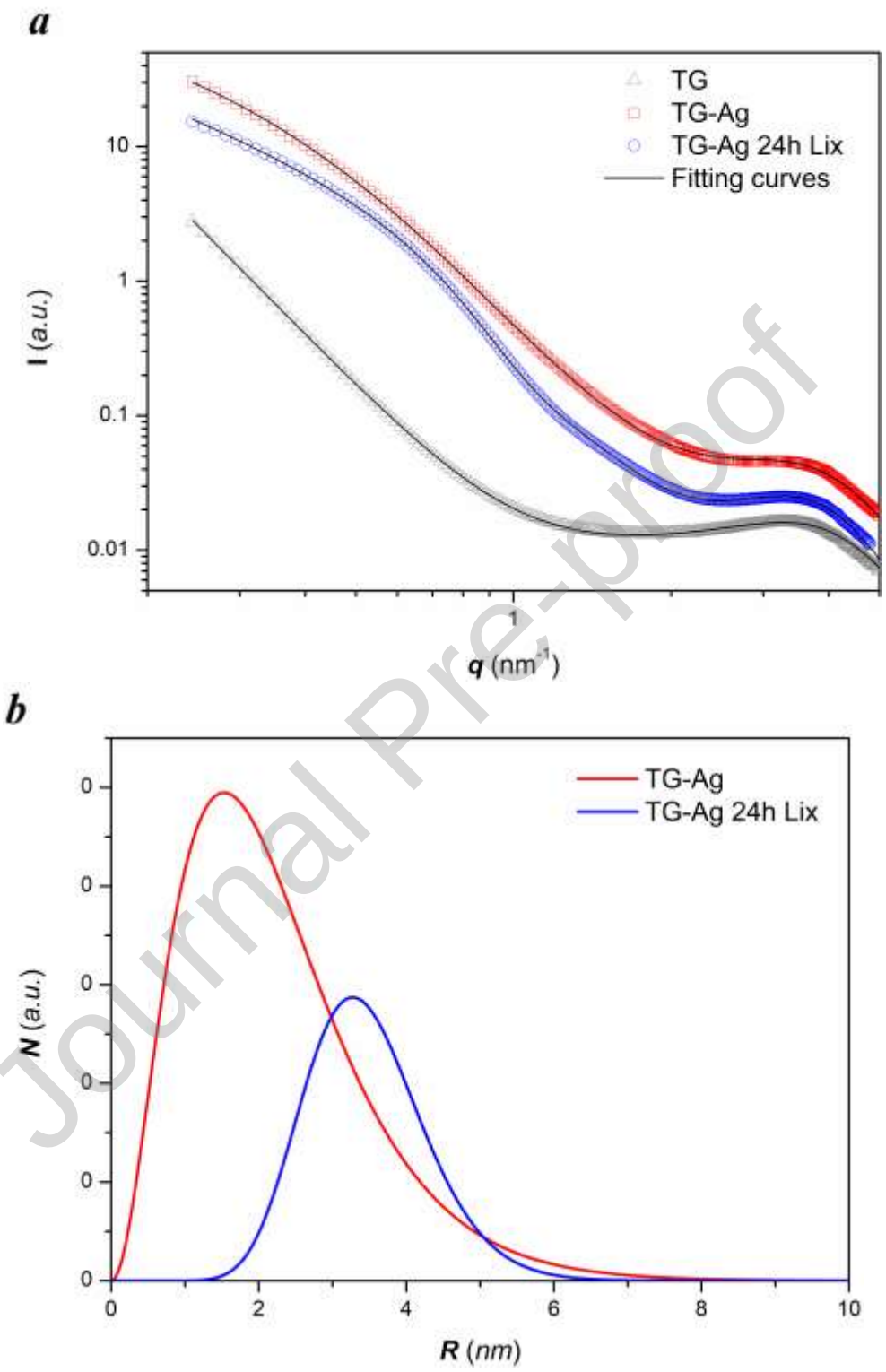

Figure 3. *a*) SAXS curves for TG and TG-Ag samples and TG-Ag sample after a 24-hour leaching process and *b*) size distribution analysis using the Schultz-Zimm model.

Figure 4 illustrates the coating surface changes using FESEM. It can be seen that the effect of inclusion of clay nanoparticles within the formulation of the precursor solutions is a key factor. Firstly, a good compatibility between the clay nanoparticles and the surrounding organic-inorganic hybrid matrix can be inferred. The figure 4 *a* shows the morphology of TGL coating at a relatively low magnification of 1500 X, in which an integer and continuous surface can be appreciated, without any noticeable microstructural irregularities; only a couple of small particles are deposited, which allows to obtain a well-focused image. When silver is present in hybrid coatings, the development of superficial particles takes place. For TG-Ag and TGL-Ag samples, Figures 4 *b* and 4 *c* respectively, an abundant spreading of nanoparticles, undoubtedly of silver, is observed. These silver nanoparticles are produced in the gel stage and grown during the thermal process of coating consolidation. The surface rise of the silver, from inner part of the coatings to the outer surface, is facilitated by the temperature and promoted by the permeability of the hybrid organic-inorganic sol-gel matrix to ionic diffusion. Once silver ions reach the external surface of the coating, they can coalesce and produce silver particles, without the size limitations offered by a solid matrix. Nevertheless, significant differences were also observed between the silver-doped coatings, depending on whether clay nanoparticles were present or not. In coatings containing clay nanoparticles, TGL-Ag sample, the development of large (microsized) silver particles was predominantly avoided, while the TG-Ag sample present such higher size particles. This difference allows the assumption that clay nanoparticles can improve the property of the coating as a silver reservoir. An excessive migration of silver ions towards the external surface of the coatings could have negative effects, exposing the superficial silver to a mechanical loss, in one hand, and inducing early depletion of the silver content of coatings, on

the other hand. Therefore, the presence of clay nanoparticles, within the silver-doped coating, could be expected to be highly beneficial for the long-term antibacterial effect.

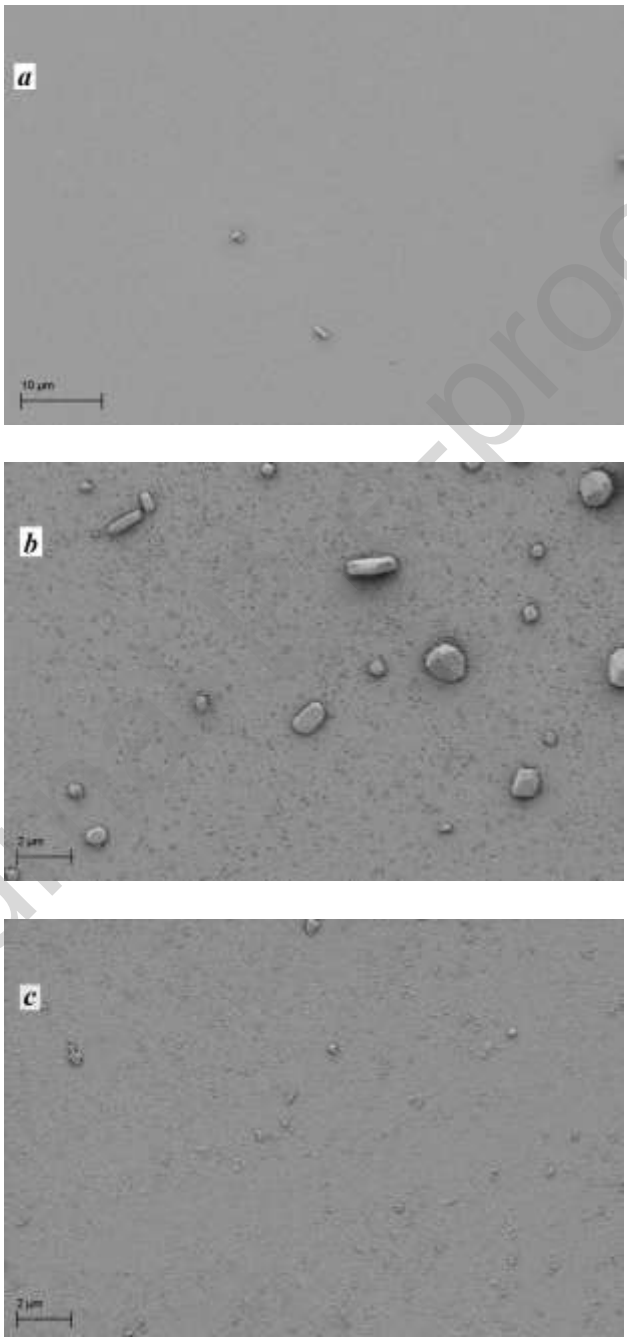

Figure 4. FESEM micrographs corresponding to the surfaces of samples: *a*) TGL, at 1500 X, *b*) TG-Ag, at 5000 X, and *c*) TGL-Ag, at 5000 X.

3.2. Silver releasing and antibacterial performance

Processes in which silver is released from a retaining medium could involve both the diffusion of free Ag^+ ions and small clusters, initially present within the coating, and the oxidative dissolution process of the silver particles embedded into the hybrid organic-inorganic structure. Such oxidative dissolution process involves the formation of an oxidized layer of Ag_2O on the surface of the metallic silver nanoparticle. Thus, the dissolution of such Ag_2O layer results in releasing Ag^+ ions. Therefore, the proposed mechanism of silver releasing may involve the following surface reactions, Eq. 4 and Eq. 5: [35]

$$2Ag_{(s)} + \frac{1}{2}O_2 \rightarrow Ag_2O_{(s)} \quad \text{Eq. 4}$$

$$Ag_2O_{(s)} + 2H^+ \rightarrow H_2O + 2Ag^+ \quad \text{Eq. 5}$$

Thus, antibacterial behavior of this kind of surface coatings will depend directly on the aggregation state of silver nanoparticles and their ability to reach its surface, where microorganisms could form colonies. Silver ions releasing, under conditions of water immersion, is highly dependent on the composition of the surface coatings and the temperature [45,46]. Figure 5 shows the silver ions releasing kinetic, determined by ICP analysis during the first eight hours of immersion in deionized water at 20 and 37 °C, for TG-Ag and TGL-Ag samples. At 20 °C (Figure 5 *a*), the silver releasing proceeds linearly. During the first hour of immersion, TG-Ag and TGL-Ag samples released silver at ratios of 0.012 ± 0.001 μg/cm^2 and 0.044 ± 0.004

$\mu g/cm^2$, respectively. Then, although silver is present in both samples at the same molecular ratio, the observed difference in their releasing rates might be attributed to the effect of clay nanoparticles on the silver nanoparticle size within the coating layer. According to shrinking particle models, the oxidative dissolution process is mainly controlled by the surface reaction and/or the mass transfer process, and then, the initial size of silver nanoparticles is a determining parameter for dissolution rate [47–50]. The smaller particle size, the faster oxidative dissolution will be. In our previous work, it was observed that clay nanoparticles limit the grow of silver particle size in the coatings layer during the thermal processing [28]. Thus, the conformation of TGL-Ag samples with smaller silver nanoparticles could be, partially, the responsible factor producing the faster dissolution process compared to samples free of clay nanoparticles [51]. As the lixiviation process is initiated at a higher temperature, the releasing kinetics are strongly modified for both TG-Ag and TGL-Ag samples. Figure 5 b illustrates the Ag^+ ions release profiles obtained at 37 °C. In this case, the releasing process of both samples, with and without clay nanoparticles, exhibit an exponential increase with liberation levels three orders of magnitude higher than those observed at 20 °C, with amounts of silver released of 11.0 ± 1.1 $\mu g/cm^2$ and 13.3 ± 1.3 $\mu g/cm^2$, during the first hour of immersion, for TG-Ag and TGL-Ag samples, respectively. This phenomenon can be explained by the dependence of the oxidative dissolution process on the resistances offered by diffusion coefficients and by the chemical reactivity of the surface of the particles [52]. At lower temperatures, the resistance offered by diffusivity of reactants is much higher than the resistance offered by the kinetic of the surface oxidation of silver nanoparticles. In contrast, at higher temperatures, diffusivity increases, its resistance drops, and the oxidative dissolution is mainly controlled by the surface oxidation of silver nanoparticles. Then, with the increase of temperature from 20 °C to 37 °C, the silver

liberation rate grows significantly, always with a faster oxidative dissolution in clay-containing samples.

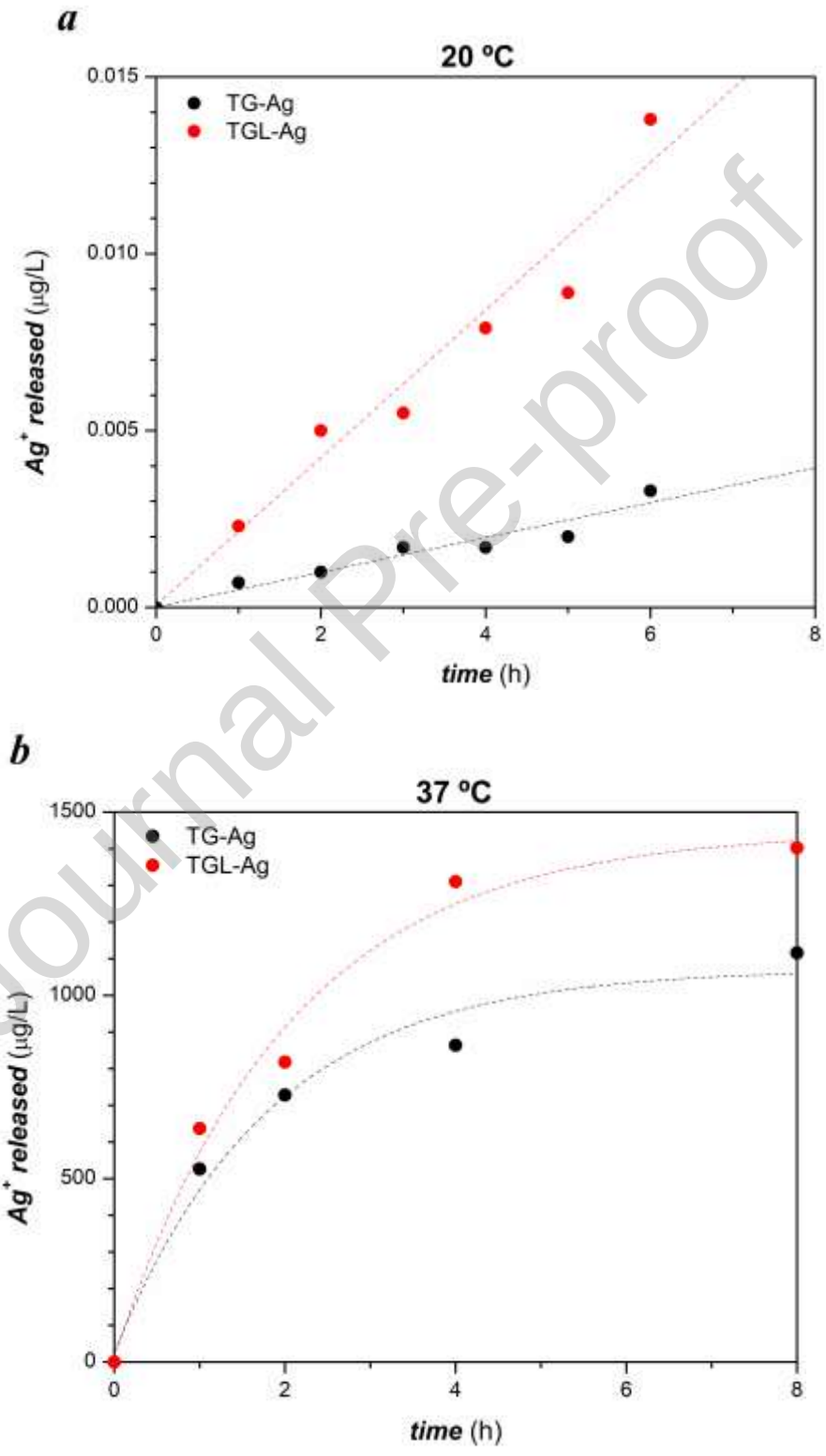

Figure 5. Time-Depletion curves of the total released silver from TG-Ag and TGL-Ag samples, estimated by ICP-OES at *a*) 20 °C and *b*) 37 °C.

Studying the variation of plasmonic bands, using UV-Vis spectroscopy, allows the detection of silver nanoparticles that fade by long-term immersion of the hybrid coatings in distilled water. Figure 6 shows the absorbance, at the maximum of the plasmonic band, as a function of immersion time, from 0 to 80 days at 37 °C. The continuous decrease of the plasmonic bands, for the TG-Ag and TGL-Ag samples, is observed as the immersion time increases. Although both samples show a gradual dissolution of silver nanoparticles, in the case of TG-Ag sample, the plasmonic surface resonance of silver nanoparticles present its highest decrease during the firsts 15 days of immersion, after which it changes more slowly. After 80 days of immersion, the UV-Vis spectra shows a small shoulder at lower wavelengths, around 380 nm, which is characteristic of large silver particles with secondary resonances [53,54]. On the other hand, TGL-Ag sample evidences a more continuous decline of its plasmonic band, almost completely disappearing after 80 days of immersion. Presumably, the narrow size distribution of silver nanoparticles shown by the TGL-Ag sample, due to the incorporation of clay nanoparticles, allowed to achieve almost complete dissolution and continuous release of silver ions. In the case of TG-Ag sample, the absence of clay nanoparticles allows for an overgrowth of silver particles, with a broader size distribution, that leads to a lesser silver releasing under immersion conditions. It is worth to note that the releasing behavior observed in TGL-Ag sample allows to ensure that all the silver embedded into the hybrid organic-inorganic structure will be able to produce antibacterial silver free ions, minimizing its inefficacy due to the formation of larger agglomerates. Figure 7 shows a picture with TGL-Ag samples before and after 80 days of immersion in DI water at 37 °C. A total vanishing of the brown color is clearly observed.

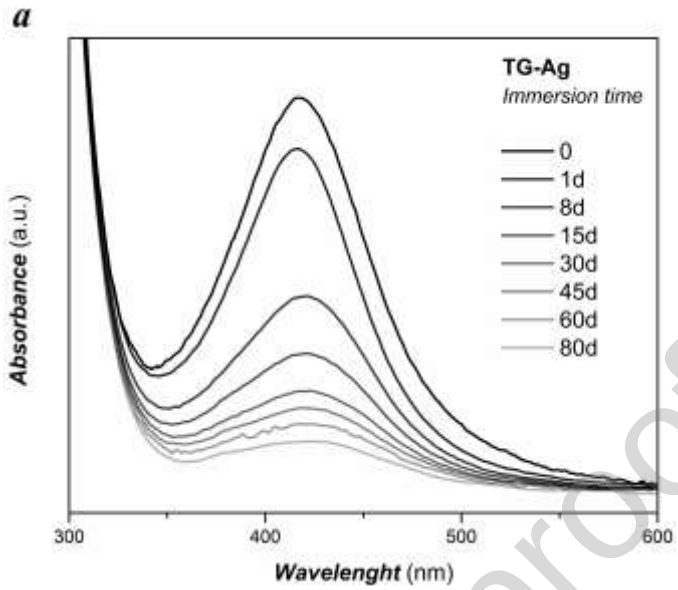

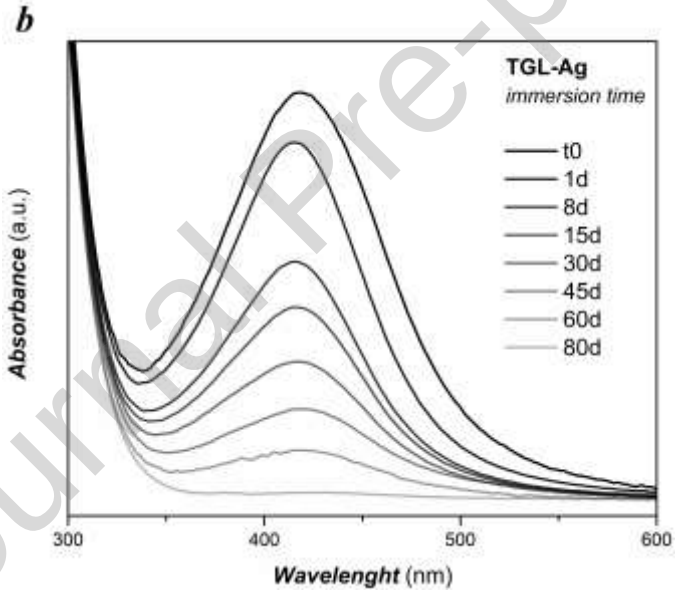

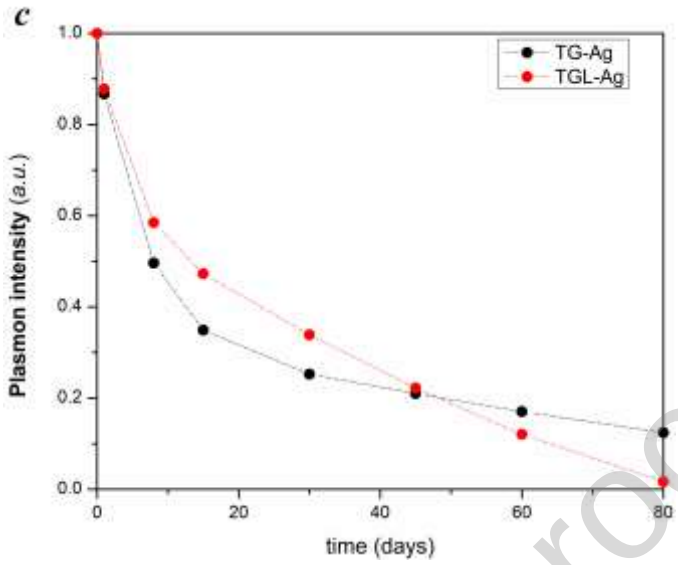

Figure 6. UV-Visible spectra of samples leached of a) TG-Ag and b) TGL-Ag at different times and c) variation of the intensity of the plasmonic band along the immersion time.

Figure 7. Photograph of TGL-Ag samples on glass substrates: original sample (*left*) and leached sample for 80 days (*right*).

Silver releasing behavior, and its biocidal performance, depends significantly on the physicochemical characteristic and the bacteriologic conditions of the environment to which the antibacterial material is exposed. Certainly, immersion of the antibacterial coating in a rich liquid medium is an extreme use condition to avoid the development of microbiologic activity. Then, the initial concentration of bacteria (OD600 values) and the rate at which silver is released are

the key factors for successfully inhibiting bacterial growth. Figure 8 shows, in terms of optical density at 600 nm (OD_{600}), the bacterial growth as a function of the initial concentration of E. coli, after immersion of the glass samples coated with the different materials. Firstly, it could be appreciated that, for silver-free coatings (TG and TGL samples), bacterial growth showed the typical *E.coli* behavior expected during the exponential growth phase and clay nanoparticles have no inhibitory effect by themselves. When silver was present, TG-Ag and TGL-Ag samples, no clear difference between the antibacterial performances of TG-Ag and TGL-Ag samples can be assumed with certainty and the inhibitory capacity of the silver-doped coatings depended on the initial bacterial inoculum. For those liquid cultures with initial OD_{600} values ranging between 0.007 to 0.03 (meaning approx. 10^6 to 10^7 cells/mL), the inhibitory effect of the silver-doped coatings was very clear, reaching maximum OD values of 0.1, or lower, and no cell growth was observed during the remaining time of the experiment, (Fig. 8 *b*, *c,* and *d*). Certainly, a near linear relationship between OD values of initial stage and Stationary Phase (*SP*) can be appreciated. Unlikely, when initial concentration of cells was around OD values of 0.1, or higher (meaning approx. 10^8 cells/mL), no inhibitory effect of silver coatings was observed on the cell growth, and cultures with silver coatings behavior was similar to the control cultures with no silver, Fig. 8 *a*. Thus, the OD_{SP} value is dependent on both the initial concentration of bacteria and on the silver release rate, the lower the initial concentration of bacteria, the better the performance of silver-doped coatings. Simultaneously with bacterial growth in the liquid medium, silver ions released from coatings increases its concentration in the experimental environment. If the initial concentration of bacteria is relatively low, released silver ions are able to stop the growing of bacteria. It is this case where the effect of clay content can be observed in the antibacterial performance; the higher silver release is appreciated by the lower OD_{SP} value

achieved. On the contrary, when the initial concentration of bacteria is relatively high, *p.e.* OD_0=0.130, independently on content of clay nanoparticles, the silver releasing process is not enough to stop the grow phase of the bacterial development in the rich medium under the conditions used during these experiments.

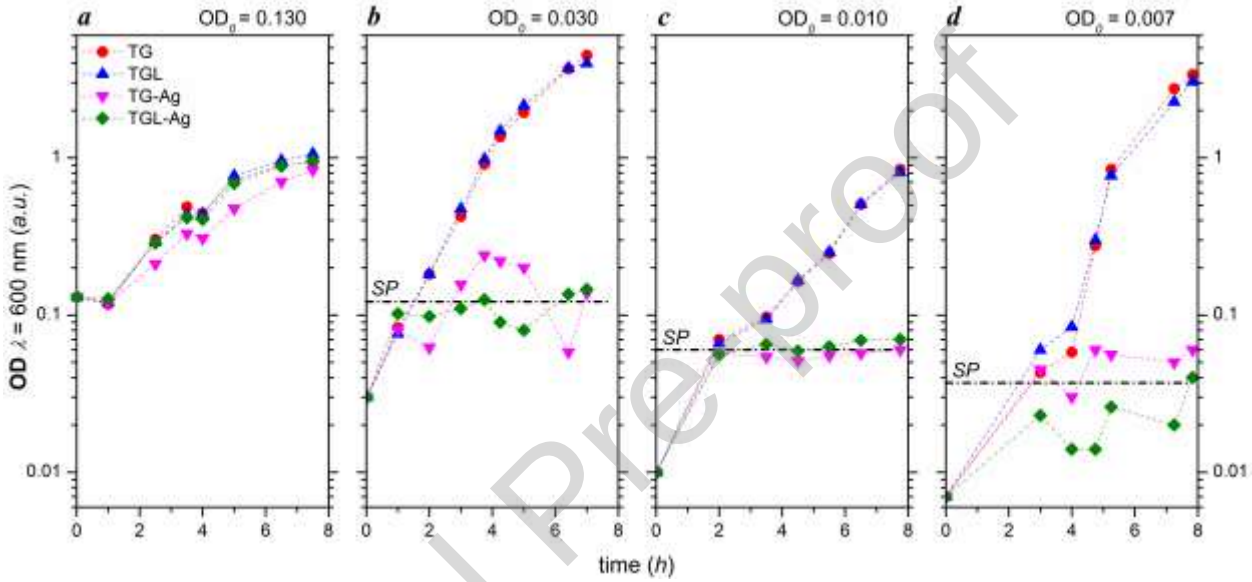

Figure 8. Growth curves in *E. coli* liquid medium in the presence hybrid samples (TG, TGL, TG-Ag and TGL-Ag), for initial inoculum of *a*) OD_{600} = 0.130, *b*) OD_{600} = 0.030, *c*) OD_{600} = 0, 010 and *d*) OD_{600} = 0.007; all incubated for 8 hours.

4. CONCLUSIONS

In this work, hybrid organic-inorganic sol-gel nanocomposite coatings were synthetized from tetraethoxysilane, 3-glycidoxypropyltrimethoxysilane and synthetic clay nanoparticles. To achieve antibacterial behavior, the coatings were doped with stabilized silver nitrate salts incorporated in the formulation of the precursor sols. Clay nanoparticles evidenced a stabilization effect in the sol stage, avoiding the formation of agglomerates, and drove the development of a narrower size distribution of silver nanoparticles within the coatings,

improving their homogeneity and the retaining of silver nanoparticles in the internal structure of coatings. Obtained coatings presented a matrix nanostructure capable of allowing ionic migration while keeping the developed silver nanoparticles retained inside the coating material. Lixiviation analysis showed that the influence of clay nanoparticles on morphology and distribution of silver nanoparticles enabled a near total and continuous silver releasing process.

Although no significant difference was observed in the inhibitory behaviour under immersion conditions, between samples with and without clay nanoparticles, its influence on size and distribution of silver nanoparticles allows to maximize the efficiency of the oxidative dissolution process and, therefore, to optimize the use of this kind of coatings as silver reservoir for biocide purposes.

AUTHOR INFORMATION

Corresponding Author

* Hugo F. Giraldo Mejía. E-mail: hugo.giraldo@amtc.uchile.cl

Present Address

† Hugo F. Giraldo Mejía. Advanced Mining Technology Center (AMTC), Universidad de Chile, Av. Tupper 2007, Santiago 8370451, Chile.

Author Contributions

The manuscript was written through contributions of all authors. All authors have given approval to the final version of the manuscript.

Funding Sources

Argentine National Agency of Scientific and Technological Promotion (ANPCyT). Projects PICT 2017 3762 and PICT 2017 1594).

Brazilian National Laboratory of Synchrotron Light (LNLS). Project 6780/10 - Proposal SAXS1 20170157.

ACKNOWLEDGMENT

Authors want to acknowledge the Argentine National Council of Scientific and Technical Research (CONICET) and to the Argentine National Agency of Scientific and Technological Promotion (ANPCyT, PICT 2017 3762 and PICT 2017 1594) and to the Brazilian National Laboratory of Synchrotron Light (LNLS, Project 6780/10, Proposal SAXS1 20170157) for the financial and technical supports. Delanta S.A., supplier of clay nanoparticles, Laponite® S482, and Mr. Martin Lere, by technical support, are also gratefully acknowledged.

REFERENCES

[1] G. Franci, A. Falanga, S. Galdiero, L. Palomba, M. Rai, G. Morelli, M. Galdiero, Silver nanoparticles as potential antibacterial agents, Molecules. 20 (2015) 8856–8874. https://doi.org/10.3390/molecules20058856.

[2] L. Sun, A.K. Singh, K. Vig, S.R. Pillai, S.R. Singh, Silver nanoparticles inhibit replication of respiratory syncytial virus, J. Biomed. Nanotechnol. 4 (2008). https://doi.org/10.1166/jbn.2008.012.

[3] L. Lu, R.W.Y. Sun, R. Chen, C.K. Hui, C.M. Ho, J.M. Luk, G.K.K. Lau, C.M. Che, Silver nanoparticles inhibit hepatitis B virus replication, Antivir. Ther. 13 (2008) 252–262.

[4] J.R. Swathy, M. Udhaya Sankar, A. Chaudhary, S. Aigal, Anshup, T. Pradeep,

Antimicrobial silver: An unprecedented anion effect, Sci. Rep. 11 (2014). https://doi.org/10.1038/srep07161.

[5] S.M. Pourmortazavi, M. Taghdiri, V. Makari, M. Rahimi-Nasrabadi, Procedure optimization for green synthesis of silver nanoparticles by aqueous extract of Eucalyptus oleosa, Spectrochim. Acta - Part A Mol. Biomol. Spectrosc. 136 (2015) 1249–1254. https://doi.org/10.1016/j.saa.2014.10.010.

[6] I. Kohsari, Z. Shariatinia, S.M. Pourmortazavi, Antibacterial electrospun chitosan-polyethylene oxide nanocomposite mats containing bioactive silver nanoparticles, Carbohydr. Polym. 140 (2016) 287–298. https://doi.org/10.1016/j.carbpol.2015.12.075.

[7] R. Heydari, M.F. Koudehi, S.M. Pourmortazavi, Antibacterial Activity of Fe3O4/Cu Nanocomposite: Green Synthesis Using Carum carvi L. Seeds Aqueous Extract, ChemistrySelect. 4 (2019) 531–535. https://doi.org/10.1002/slct.201803431.

[8] I. Kohsari, M. Mohammad-Zadeh, S. Minaeian, M. Rezaee, A. Barzegari, Z. Shariatinia, M.F. Koudehi, S. Mirsadeghi, S.M. Pourmortazavi, In vitro antibacterial property assessment of silver nanoparticles synthesized by Falcaria vulgaris aqueous extract against MDR bacteria, J. Sol-Gel Sci. Technol. 90 (2019) 380–389. https://doi.org/10.1007/s10971-019-04961-0.

[9] H.V. Tran, L.D. Tran, C.T. Ba, H.D. Vu, T.N. Nguyen, D.G. Pham, P.X. Nguyen, Synthesis, characterization, antibacterial and antiproliferative activities of monodisperse chitosan- based silver nanoparticles, Colloids Surfaces A Physicochem. Eng. Asp. 360 (2010) 32–40. https://doi.org/10.1016/j.colsurfa.2010.02.007.

[10] Y. Zhang, X. Cheng, Y. Zhang, X. Xue, Y. Fu, Biosynthesis of silver nanoparticles at room temperature using aqueous aloe leaf extract and antibacterial properties, Colloids Surfaces A Physicochem. Eng. Asp. 423 (2013) 63–68. https://doi.org/10.1016/j.colsurfa.2013.01.059.

[11] K. Hileuskaya, A. Ladutska, V. Kulikouskaya, A. Kraskouski, G. Novik, I. Kozerozhets, A. Kozlovskiy, V. Agabekov, 'Green' approach for obtaining stable pectin-capped silver nanoparticles: Physico-chemical characterization and antibacterial activity, Colloids

Surfaces A Physicochem. Eng. Asp. 585 (2020) 124141. https://doi.org/10.1016/j.colsurfa.2019.124141.

[12] S. Kumar, M. Singh, D. Halder, A. Mitra, Mechanistic study of antibacterial activity of biologically synthesized silver nanocolloids, Colloids Surfaces A Physicochem. Eng. Asp. 449 (2014) 82–86. https://doi.org/10.1016/j.colsurfa.2014.02.027.

[13] H. Haidari, N. Goswami, R. Bright, Z. Kopecki, A.J. Cowin, S. Garg, K. Vasilev, The interplay between size and valence state on the antibacterial activity of sub-10 nm silver nanoparticles, Nanoscale Adv. 1 (2019) 2365–2371. https://doi.org/10.1039/c9na00017h.

[14] S. Tang, J. Zheng, Antibacterial Activity of Silver Nanoparticles: Structural Effects, Adv. Healthc. Mater. 7 (2018). https://doi.org/10.1002/adhm.201701503.

[15] M.H. Shirangi, X.J. Fan, B. Michel, Mechanism of moisture diffusion, hygroscopic swelling and adhesion degradation in Epoxy Molding Compounds, in: Proc. - 2008 Int. Symp. Microelectron. IMAPS 2008, 2008: pp. 1082–1089. https://doi.org/10.1007/978-1-4419-5719-1_2.

[16] H. Ardebili, E.H. Wong, M. Pecht, Hygroscopic swelling and sorption characteristics of epoxy molding compounds used in electronic packaging, IEEE Trans. Components Packag. Technol. 26 (2003) 206–214. https://doi.org/10.1109/TCAPT.2002.806172.

[17] G.E. Guloglu, M.C. Altan, Moisture Absorption of Carbon/Epoxy Nanocomposites, J. Compos. Sci. 4 (2020) 21. https://doi.org/10.3390/jcs4010021.

[18] R. Procaccini, A. Bouchet, J.I. Pastore, C. Studdert, S. Ceré, S. Pellice, Silver-functionalized methyl-silica hybrid materials as antibacterial coatings on surgical-grade stainless steel, Prog. Org. Coatings. 97 (2016) 28–36. https://doi.org/10.1016/j.porgcoat.2016.03.012.

[19] R.A. Procaccini, C.A. Studdert, S.A. Pellice, Silver doped silica-methyl hybrid coatings. Structural evolution and antibacterial properties, Surf. Coatings Technol. 244 (2014) 92–97. https://doi.org/10.1016/j.surfcoat.2014.01.036.

[20] R. Procaccini, S. Ceré, S. Pellice, Development and thermal evolution of silver clusters in

hybrid organic-inorganic sol-gel coatings, Surf. Coatings Technol. 205 (2011) 5464–5469. https://doi.org/10.1016/j.surfcoat.2011.06.018.

[21] H. Miyoshi, H. Ohno, K. Sakai, N. Okamura, H. Kourai, Characterization and photochemical and antibacterial properties of highly stable silver nanoparticles prepared on montmorillonite clay in n-hexanol, J. Colloid Interface Sci. 345 (2010) 433–441. https://doi.org/10.1016/j.jcis.2010.01.034.

[22] M.G. Olivier, M. Fedel, V. Sciamanna, C. Vandermiers, C. Motte, M. Poelman, F. Deflorian, Study of the effect of nanoclay incorporation on the rheological properties and corrosion protection by a silane layer, Prog. Org. Coatings. 72 (2011) 15–20. https://doi.org/10.1016/j.porgcoat.2010.11.022.

[23] R. Herrera Alonso, L. Estevez, H. Lian, A. Kelarakis, E.P. Giannelis, Nafion-clay nanocomposite membranes: Morphology and properties, Polymer (Guildf). 50 (2009) 2402–2410. https://doi.org/10.1016/j.polymer.2009.03.020.

[24] F. Deflorian, S. Rossi, M. Fedel, C. Motte, Electrochemical investigation of high-performance silane sol-gel films containing clay nanoparticles, Prog. Org. Coatings. 69 (2010) 158–166. https://doi.org/10.1016/j.porgcoat.2010.04.007.

[25] P.A. Wheeler, J. Wang, J. Baker, L.J. Mathias, Synthesis and characterization of covalently functionalized laponite clay, Chem. Mater. 17 (2005) 3012–3018. https://doi.org/10.1021/cm050306a.

[26] I. Santana, A. Pepe, W. Schreiner, S. Pellice, S. Ceré, Hybrid sol-gel coatings containing clay nanoparticles for corrosion protection of mild steel, Electrochim. Acta. 203 (2016) 396–403. https://doi.org/10.1016/j.electacta.2016.01.214.

[27] V. Dalmoro, J.H.Z. dos Santos, E. Armelin, C. Alemán, D.S. Azambuja, Sol-gel hybrid films based on organosilane and montmorillonite for corrosion inhibition of AA2024, J. Colloid Interface Sci. 426 (2014) 308–313. https://doi.org/10.1016/j.jcis.2014.04.021.

[28] H.F. Giraldo Mejía, L. Yohai, A. Pedetta, K. Herrera Seitz, R.A. Procaccini, S.A. Pellice, Epoxy-silica/clay nanocomposite for silver-based antibacterial thin coatings: Synthesis

and structural characterization, J. Colloid Interface Sci. 508 (2017) 332–341. https://doi.org/10.1016/j.jcis.2017.08.058.

[29] T.C. Huang, H. Toraya, T.N. Blanton, Y. Wu, X-ray powder diffraction analysis of silver behenate, a possible low-angle diffraction standard, J. Appl. Crystallogr. 26 (1993) 180–184. https://doi.org/10.1107/S0021889892009762.

[30] A.P. Hammersley, FIT2D: A multi-purpose data reduction, analysis and visualization program, J. Appl. Crystallogr. 49 (2016) 646–652. https://doi.org/10.1107/S1600576716000455.

[31] I. Breßler, J. Kohlbrecher, A.F. Thünemann, SASfit: A tool for small-angle scattering data analysis using a library of analytical expressions, J. Appl. Crystallogr. 48 (2015) 1587–1598. https://doi.org/10.1107/S1600576715016544.

[32] M. Teubner, R. Strey, Origin of the scattering peak in microemulsions, J. Chem. Phys. 87 (1987) 3195–3200. https://doi.org/10.1063/1.453006.

[33] P. Debye, H.R. Anderson, H. Brumberger, Scattering by an inhomogeneous solid. II. the correlation function and its application, J. Appl. Phys. 28 (1957) 679–683. https://doi.org/10.1063/1.1722830.

[34] T. Zemb, P. Lindner, Neutron, X-rays and Light. Scattering Methods Applied to Soft Condensed Matter, 2002. https://doi.org/10.1016/s1369-7021(02)01143-4.

[35] Z. Adamczyk, M. Oćwieja, H. Mrowiec, S. Walas, D. Lupa, Oxidative dissolution of silver nanoparticles: A new theoretical approach, J. Colloid Interface Sci. 469 (2016) 355–364. https://doi.org/10.1016/j.jcis.2015.12.051.

[36] J. Liu, R.H. Hurt, Ion release kinetics and particle persistence in aqueous nano-silver colloids, Environ. Sci. Technol. 44 (2010) 2169–2175. https://doi.org/10.1021/es9035557.

[37] T.Y. Cath, A.E. Childress, M. Elimelech, Forward osmosis: Principles, applications, and recent developments, J. Memb. Sci. 281 (2006) 70–87. https://doi.org/10.1016/j.memsci.2006.05.048.

[38] J. Liu, D.A. Sonshine, S. Shervani, R.H. Hurt, Controlled release of biologically active silver from nanosilver surfaces, ACS Nano. 4 (2010) 6903–6913. https://doi.org/10.1021/nn102272n.

[39] Z.M. Xiu, J. Ma, P.J.J. Alvarez, Differential effect of common ligands and molecular oxygen on antimicrobial activity of silver nanoparticles versus silver ions, Environ. Sci. Technol. 45 (2011) 9003–9008. https://doi.org/10.1021/es201918f.

[40] B. Molleman, T. Hiemstra, Time, pH, and size dependency of silver nanoparticle dissolution: The road to equilibrium, Environ. Sci. Nano. 4 (2017) 1314–1327. https://doi.org/10.1039/c6en00564k.

[41] P.R. Laity, J.E. Taylor, S.S. Wong, P. Khunkamchoo, K. Norris, M. Cable, G.T. Andrews, A.F. Johnson, R.E. Cameron, A review of small-angle scattering models for random segmented poly(ether-urethane) copolymers, Polymer (Guildf). 45 (2004) 7273–7291. https://doi.org/10.1016/j.polymer.2004.08.033.

[42] S. Peng, Q. Guo, T.C. Hughes, P.G. Hartley, In situ synchrotron SAXS study of polymerizable microemulsions, Macromolecules. 44 (2011) 3007–3015. https://doi.org/10.1021/ma102978u.

[43] D.R. Vollet, W.C. De Castro, D.A. Donatti, A.I. Ruiz, Small-angle X-ray scattering and nitrogen adsorption study of the nanoporosity elimination in TEOS sonohydrolysis-derived xerogels, Phys. Status Solidi Appl. Mater. Sci. 202 (2005) 411–418. https://doi.org/10.1002/pssa.200406929.

[44] C. Gommes, S. Blacher, B. Goderis, R. Pirard, B. Heinrichs, C. Alié, J.P. Pirard, In situ SAXS analysis of silica gel formation with an additive, J. Phys. Chem. B. 108 (2004) 8983–8991. https://doi.org/10.1021/jp049568a.

[45] K. Loza, J. Diendorf, C. Sengstock, L. Ruiz-Gonzalez, J.M. Gonzalez-Calbet, M. Vallet-Regi, M. Köller, M. Epple, The dissolution and biological effects of silver nanoparticles in biological media, J. Mater. Chem. B. 2 (2014) 1634–1643. https://doi.org/10.1039/c3tb21569e.

[46] O. Akhavan, Lasting antibacterial activities of Ag-TiO2/Ag/a-TiO2 nanocomposite thin film photocatalysts under solar light irradiation, J. Colloid Interface Sci. 336 (2009) 117–124. https://doi.org/10.1016/j.jcis.2009.03.018.

[47] A.J. McCarthy, The Mechanism of the Oxidative Dissolution of Colloidal Gold in Cyanide Media, J. Electrochem. Soc. 145 (1998) 408. https://doi.org/10.1149/1.1838278.

[48] H. Grénman, T. Salmi, D.Y. Murzin, Solid-liquid reaction kinetics - Experimental aspects and model development, Rev. Chem. Eng. 27 (2011) 53–77. https://doi.org/10.1515/REVCE.2011.500.

[49] I. Rivera, F. Patiño, A. Roca, M. Cruells, Kinetics of metallic silver leaching in the O2-thiosulfate system, Hydrometallurgy. 156 (2015) 63–70. https://doi.org/10.1016/j.hydromet.2015.05.009.

[50] G. Alvarado-Macías, J.C. Fuentes-Aceituno, F. Nava-Alonso, J.C. Lee, Silver leaching with the nitrite-copper novel system: A kinetic study, Hydrometallurgy. 160 (2016) 98–105. https://doi.org/10.1016/j.hydromet.2015.12.014.

[51] Q. Lin, D.J. Barker, K.J. Dobson, P.D. Lee, S.J. Neethling, Modelling particle scale leach kinetics based on X-ray computed micro-tomography images, Hydrometallurgy. 162 (2016) 25–36. https://doi.org/10.1016/j.hydromet.2016.02.008.

[52] V. Safari, G. Arzpeyma, F. Rashchi, N. Mostoufi, A shrinking particle-shrinking core model for leaching of a zinc ore containing silica, Int. J. Miner. Process. 93 (2009) 79–83. https://doi.org/10.1016/j.minpro.2009.06.003.

[53] D.D. Evanoff, G. Chumanov, Size-controlled synthesis of nanoparticles. 1. “silver-only” aqueous suspensions via hydrogen reduction, J. Phys. Chem. B. 108 (2004) 13948–13956. https://doi.org/10.1021/jp047565s.

[54] D.K. Bhui, H. Bar, P. Sarkar, G.P. Sahoo, S.P. De, A. Misra, Synthesis and UV-vis spectroscopic study of silver nanoparticles in aqueous SDS solution, J. Mol. Liq. 145 (2009) 33–37. https://doi.org/10.1016/j.molliq.2008.11.014.

Credit Author Statement

Hugo F. Giraldo Mejía: Conceptualization, Methodology, Investigation, Data Curation, Validation, Writing- Original draft preparation, Writing- Reviewing and Editing. **Karina Herrera Seitz:** Methodology, Investigation, Writing- Original draft preparation, Writing- Reviewing and Editing. **Matías Valdés:** Methodology, Investigation, Writing- Original draft preparation, Writing- Reviewing and Editing. **Abdusalam Uheida:** Methodology, Investigation, Writing- Original draft preparation, Writing- Reviewing and Editing. **Raúl A. Procaccini:** Funding acquisition, Supervision, Conceptualization, Methodology, Investigation, Writing- Original draft preparation, Writing- Reviewing and Editing. **Sergio A. Pellice:** Funding acquisition, Project administration, Supervision, Conceptualization, Methodology, Investigation, Writing- Original draft preparation, Writing- Reviewing and Editing.

Declaration of interests

☒The authors declare that they have no known competing financial interests or personal relationships that could have appeared to influence the work reported in this paper.

☐The authors declare the following financial interests/personal relationships which may be considered as potential competing interests:

Graphical abstract

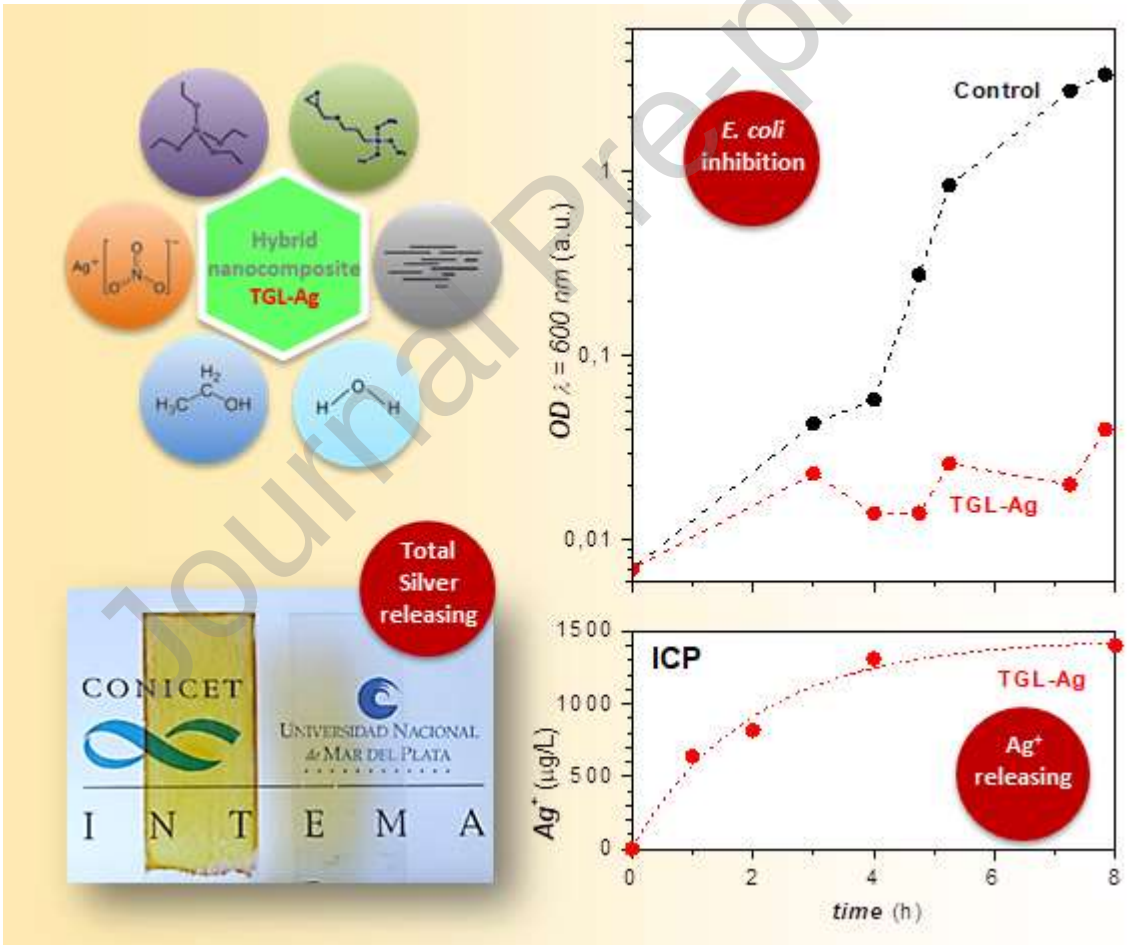

Highlights

- Hybrid matrix works as a silver nanoparticle reservoir.
- Sol-gel made hybrid nanostructure offer a permeable pathway to ionic diffusion.
- Clay nanoparticles contribute to regulate the silver nanoparticle size.
- Oxidative Dissolution Process progress until complete silver releasing.